Macrophage migration inhibitory factor in inflammasome formation and macrophage recruitment by cervical squamous cell carcinoma cells

QIANQIAN ZHANG, MENGXIN WANG and SUHUI WU

Department of Obstetrics and Gynecology, Third Hospital of Shanxi Medical University, Shanxi Bethune Hospital, Shanxi Academy of Medical Sciences, Tongji Shanxi Hospital, Taiyuan, Shanxi 030032, P.R. China

Received September 4, 2024; Accepted December 6, 2024

DOI: 10.3892/ol.2025.14910

Abstract. Despite the demonstrated efficacy of immune checkpoint blockade therapies in various types of cancer, their efficacy in cervical cancer is limited. A crucial pro-inflammatory cytokine, macrophage migration inhibitory factor (MIF), is highly expressed in various types of cancers and contributes to tumor progression via the regulation of inflammatory responses and the tumor microenvironment. The present study aimed to explore the role of MIF in cervical squamous cell carcinoma (CSCC). Western blotting, reverse transcription-quantitative polymerase chain reaction, Cell-Counting Kit-8, flow cytometry and enzyme-linked immunosorbent assays were used to investigate the effects of MIF on CSCC progression and in the formation of inflammasomes using SiHa cells. Transcriptome and proteome sequencing were combined to screen for key effector proteins of MIF. Moreover, *in vitro* co-culture experiments were used to evaluate the roles of MIF and TSC22 domain family protein 3 (TSC22D3) as inflammatory tumor-promoting factors in macrophage recruitment and polarization induction. The results indicated that MIF was highly expressed in CSCC with lymph node metastasis, positively associated with cervical cancer stage, and associated with a poor prognosis. MIF was also found to promote the progression of CSCC cells and to be associated with inflammasome activation. Multi-omics screening results indicated that TSC22D3 may be an important MIF interacting factor. Moreover, MIF and TSC22D3 facilitated inflammasome activation, THP-1 cell migration and M2 polarization. Therefore, it is suggested that MIF and TSC22D3 may induce macrophage infiltration in cervical cancer lesions and affect the tumor microenvironment by polarizing macrophages toward the M2 phenotype, thereby promoting CSCC progression. The present study highlights the potential of the MIF-TSC22D3 axis as a novel therapeutic target, which could conceivably help to improve the efficacy of immunotherapy in the treatment of recurrent or metastatic cervical cancer.

Correspondence to: Professor Suhui Wu, Department of Obstetrics and Gynecology, Third Hospital of Shanxi Medical University, Shanxi Bethune Hospital, Shanxi Academy of Medical Sciences, Tongji Shanxi Hospital, 99 Longcheng Street, Xiaodian, Taiyuan, Shanxi 030032, P.R. China
Email: shwu1215@163.com

Abbreviations: CSCC, cervical squamous cell carcinoma; IL, interleukin; MIF, macrophage migration inhibitory factor; RT-qPCR, reverse transcription-quantitative polymerase chain reaction; TSC22D3, TSC22 domain family protein 3

Key words: cervical cancer, inflammasome, macrophage, migration inhibitory factor, TSC22D3

Introduction

Cervical cancer is a significant public health challenge, ranking as the fourth most common type of cancer and the fourth most prevalent cause of mortality among women globally (1). The prognosis for recurrent or metastatic cervical cancer remains poor owing to limited treatment options (2-4). Despite the notable success of immune checkpoint blockade therapy in the treatment of various tumors, its clinical efficacy in recurrent or metastatic cervical cancer is suboptimal, and the factors contributing to this limited efficacy include the necessity of programmed death-ligand 1 expression, the emergence of drug resistance, and low remission rates (5,6).

Macrophage migration inhibitory factor (MIF) has been found to be highly expressed in various types of solid tumors, and to function as a multifunctional pro-inflammatory cytokine that modulates immune responses, exacerbates inflammation, and promotes cancer progression and metastasis (7). MIF regulates inflammatory pathways by directly or indirectly modulating the secretion of various cytokines, including tumor necrosis factor-α, interferon-γ, interleukin (IL)-1β and IL-18 (7). By recruiting immune cells to form an immunosuppressive tumor microenvironment, MIF provides a favorable microenvironment for cancer progression (8,9).

Inflammasomes have emerged as a key focus of research, which has advanced the understanding of tumor-associated inflammation. Inflammasomes are multiprotein complexes that detect dangerous external stimuli and initiate inflammatory responses (10). At present, the most extensively studied inflammasome is NLR family pyrin domain containing 3 (NLRP3);

it assembles into an inflammasome through self-oligomerization, activates caspase-1, and facilitates the maturation and release of IL-1β and IL-18, which recruit immunosuppressive cells (11). MIF has been indicated to influence the activation and/or assembly of the NLRP3 inflammasome through intracellular and extracellular pathways (12,13). However, the role of MIF in relation to the inflammasome in cervical cancer remains unexplored.

Initial screening via the gene chip sequencing of cervical squamous cell carcinoma (CSCC) tissues revealed the significant upregulation of MIF expression in patients with lymph node metastases (14). Therefore, the present study aimed to explore the role of MIF in the recurrence and metastasis of CSCC, which may have important clinical implications for the treatment and prevention of cervical cancer progression.

Materials and methods

Human tissue specimens. A total of 12 fresh tissue samples from patients with CSCC, with or without lymph node metastases, were collected during gynecological treatments at the Third Hospital of Shanxi Medical University (Taiyuan, China) during the period from June 2024 to August 2024. All selected patients did not have any other systemic malignant tumors, had not undergone surgery for any reason, and had no other comorbidities. In addition, they had not received any preoperative radiation or chemotherapy for CSCC, and their clinical, imaging and pathological data, and follow-up information were complete. Each sample underwent independent assessment and diagnosis by three senior clinical pathologists. After surgical removal, the fresh tissue specimens were promptly frozen and preserved in the biological specimen repository at the hospital. Written informed consent was obtained from patients and their families for the use of their samples and data, and the study protocol was approved by the Ethics Committee of the Third Hospital of Shanxi Medical University (approval no. YXLL-2024-117).

Cell culture. The human CSCC cell lines SiHa (cat. no. TCHu113; https://www.cellbank.org.cn/search-detail.php?id=187) and CaSki (cat. no. TCHu137; https://www.cellbank.org.cn/search-detail.php?id=210), both of which are human papillomavirus 16 positive, were obtained from The Cell Bank of Type Culture Collection of The Chinese Academy of Sciences. The H8 human normal cervical epithelial cell line (cat. no. TCH-C616; https://www.cas9x.com/bdxb/106381.html) was obtained from the Haixing Biosciences. The THP-1 human monocytic leukemia cell line (cat. no. CL-0233) was sourced from Wuhan Pricella Biotechnology Co., Ltd. The SiHa and CaSki cell lines are immortalized cell lines derived from cervical cancer tissues. The SiHa and CaSki cell lines were utilized at the 5th passage after purchase. SiHa and H8 cells were cultured in DMEM (cat. no. PYG0073; Boster Biological Technology) supplemented with 10% FBS (cat. no. PYG0109-500; Boster Biological Technology) and 1% antibiotics (penicillin-streptomycin). CaSki and THP-1 cell lines were cultured in RPMI-1640 medium (cat. no. PYG0006; Boster Biological Technology) supplemented with 10% FBS and 1% antibiotics. All cell lines were maintained in a cell culture incubator at 37˚C with 95% air and 5% CO_2. Cells were cultured in a 6-well plate, ensuring that the cell count reached ~1x10^6 and the confluence reached 70-80% before using the cells for subsequent experiments. THP-1 cells were used as they are widely used in scientific research as a model for studying macrophage function and differentiation. THP-1 cells are a cell line derived from human acute monocytic leukemia, and they have the potential to differentiate into macrophage-like cells, making them an important tool for studying the biological characteristics, functions and drug effects on macrophages. Due to their easy cultivation, rapid proliferation and the ability to be induced to differentiate under specific stimulation conditions, THP-1 cells have become a commonly used cell model for studying macrophage-related diseases (15).

Collection of cell culture supernatant. The culture flask was gently shaken to mix the cell culture supernatant uniformly. An appropriate amount of cell culture supernatant was carefully aspirated into a new centrifuge tube, and an appropriate amount of fresh medium added to the culture flask. The aspirated culture supernatant was centrifuged at 4˚C and 1,000 x g for 10 min, and then the supernatant was re-aspirated into a new spare centrifuge tube, discarding the remaining cell debris and impurities in the tube. The re-collected cell culture supernatant was filtered through a virus filter (0.22 μm). The filtered cell culture supernatant samples were stored at -20˚C or -80˚C to avoid repeated freeze-thaw cycles. Before use, the samples were thawed and the required medium was prepared for the experiment according to the following ratio: Conditioned medium:fresh medium=1:1.

Co-culture experiment. THP-1 cells with good growth status and a density of 80-90% were selected. After digestion and counting, the cells were added to RPMI-1640 complete medium to achieve a concentration of 5x10^5 cells/Ml. next, 100 ng/ml PMA was added, and the mixture was thoroughly mixed by pipetting. The cells were plated into a six-well plate and incubated in a cell incubator with 5% CO_2 at 37˚C for 24 h. After 24 h, the supernatant was discarded, and the cells were washed three times with PBS. RPMI-1640 complete medium was added to allow the cells to recover for another 24 h. Subsequently, the supernatant was removed again, and the cells were washed three times with PBS. The previously collected Cell Culture Supernatant was then used as the co-culture conditioned medium, added to the six-well plate and supplemented with RPMI-1640 complete medium to a total volume of 2 ml per well. The cells were co-cultured for 24 h and prepared for subsequent experiments.

Reverse-transcription quantitative PCR (RT-qPCR). Cells were cultured in a 6-well plate, until the cell count reached ~1x10^6, with a cell density of 70-80%. At this point, the cells were ready for analysis. Total RNA was extracted from cells and tissue samples using Total RNA Extraction Kit (cat. no. R1200; Beijing Solarbio Science & Technology Co., Ltd.). For mRNA quantification, the RNA was reverse transcribed into cDNA using a Reverse Transcription kit (cat. no. R223-01; Vazyme Biotech Co., Ltd.) according to the manufacturer's protocol. Subsequently, qPCR was performed using a Real-Time PCR kit (cat. no. Q711-02; Vazyme Biotech Co., Ltd.) according to the manufacturer's

protocol. The thermocycling conditions were: Initial denaturation at 95˚C for 30 sec; 40 cycles of 95˚C for 3 sec and 60˚C for 10 sec; and a final melting curve stage at 95˚C for 15 sec, 60˚C for 30 sec and 95˚C for 15 sec. The relative mRNA expression levels were normalized to those of GAPDH using the $2^{-\Delta\Delta Cq}$ method (16). The sequences of the primers used for amplification were: GAPDH forward, 5'-TGACTTCAACAGCGACACCCA-3' and reverse, 5'-CACCCTGTTGCTGTAGCCAAA-3'; MIF forward, 5'-ACCAGCTCATGGCCTTCGG-3' and reverse, 5'-TTGGCCGCGTTCATGTCG-3'; NLRP3 forward, 5'-TGAACAGCCACCTCACTT-3' and reverse, 5'-CAACCACAATCTCCGAAT-3'; apoptosis-associated speck-like protein containing a CARD (ASC) forward, 5'-TGGACGCCTTGGACCTCA-3' and reverse, 5'-TTGGCTGCCGACTGAGGA-3'; caspase-1 forward, 5'-ATTACAGACAAGGGTGCT-3' and reverse, 5'-GAATAACGGAGTCAATCAAA-3'; prostate stem cell antigen (PSCA) forward, 5'-AGCCCAGGTGAGCAACGA-3' and reverse, 5'-TCATCCACGCAGTTCAAGC-3'; laminin subunit β 1 (LAMB1) forward, 5'-TACACCTCCTCTGATAGCG-3' and reverse, 5'-ATCTCCTGAACCTCCCAC-3'; solute carrier 39 member 10 (SLC39A10) forward, 5'-TGCCTCATTTGTTTGCTG-3' and reverse, 5'-TTCCACGATGCTGTCTGT-3'; solute carrier 35 member F2 (SLC35F2) forward, 5'-TGGACTCTTTCTGTTTGGCTAT-3' and reverse, 5'-GGAGGCACGCTGCTTTCA-3'; solute carrier family 1 member 4 (SLC1A4) forward, 5'-CCATTGGGCTGCCTACTC-3' and reverse, 5'-CCTTTCTTTGTTGCCTTCTG-3'; ArfGAP with coiled-coil, ankyrin repeat and PH domain-containing protein 3 (ACAP3) forward, 5'-AGGGCGACACCGTCATCT-3' and reverse, 5'-TTCCGCACATCCTCTTTGA-3'; oxysterol binding protein like 6 (OSBPL6) forward, 5'-TCACTGTCTCAGGCACTC-3' and reverse, 5'-TCTCATTGGCTACTTGCT-3'; TSCC22 domain family protein 3 (TSC22D3) forward, 5'-CACCCTGTTGAAGACCCT-3' and reverse, 5'-TTACACCGCAGAACCACC-3'; asparagine synthetase (ASNS) forward, 5'-AACAGTTCGTGCTTCAGT-3' and reverse, 5'-ATGTAACCCTGCGTAAGT-3'; coagulation factor III (F3) forward, 5'-CCGACGAGATTGTGAAGG-3' and reverse, 5'-TGGCTGTCCGAGGTTTGT-3'; tribbles pseudokinase 3 (TRIB3), forward 5'-GCGGTTGGAGTTGGATGA-3' and reverse, 5'-GCCACAGCAGTTGCACGA-3'; inducible nitric oxide synthase (iNOS) forward, 5'-ACATGGCTCAACAGCCTGAA-3' and reverse, 5'-CCAAACACCAAGGTCATGCG-3'; arginase 1 (Arg1) forward, 5'-AATCCTGGCACATCGGGAATC-3' and reverse, 5'-TCCTGGTACATCTGGGAACTTTC-3'; CD86 forward, 5'-ATTTGGAACCAAGCAAGAGCA-3' and reverse, 5'-TACTCAGTCCCATAGTGCTGTCAC-3'; CD206 forward, 5'-ACCTCACAAGTATCCACACCATC-3' and reverse, 5'-CTTTCATCACCACACAATCCTC-3'. Each experimental condition was replicated in three separate assays.

Western blotting. The tissue was removed from liquid nitrogen, and a piece about the size of a soybean was quickly cut and placed in an Eppendorf tube. This was rinsed 2-3 times with pre-cooled sterile PBS. An appropriate volume of RIPA buffer (cat. no. AR0105; Boster Biological Technology), phosphatase inhibitor and protease inhibitor (cat. no. P1045-1; Beyotime Biotechnology) was added in a ratio of 100:1:1. The mixture was ground thoroughly on ice and then placed on a shaker to allow for complete lysis for 30 min for use (with ice added). Cells were cultured in a 6-well plate until the cell count reached ~$1x10^6$, with a cell density of 70-80%. Total protein was then extracted from the cells using RIPA buffer and quantified using a BCA Protein Assay kit (cat. no. AR118; Boster Biological Technology). SDS gels were prepared using a PAGE Gel Fast Preparation Kit (cat. no. AR0138; Boster Biological Technology). Following SDS-PAGE (typically using a gel with a concentration of 10% and loading 25 μg of sample per lane), the resolved proteins were transferred to PVDF membranes (cat. no. AR0136-04; Boster Biological Technology) and blocked using a protein-free rapid blocking solution (cat. no. AR0041; Boster Biological Technology) for 10 min at 25˚C. The membranes were subsequently incubated with a primary antibody overnight at 4˚C. The following primary antibodies were used: Anti-MIF (1:1,000 dilution; cat. no. DF6404; Affinity Biosciences), anti-GAPDH (1:3,000; cat. no. AP0063; Bioworld Technology, Inc.), anti-NLRP3 (1:1,000; cat. no. ab263899; Abcam), anti-ASC (1:1,000; cat. no. ab283684; Abcam), anti-caspase-1 (1:1,000; cat. no. ab207802; Abcam) and anti-TSC22D3 (1:2,000; cat. no. DF10077; Affinity Biosciences). After washing, the membranes were incubated with horseradish peroxidase-labeled goat anti-rabbit secondary antibody (1:3,000; cat. no. S0001; Affinity Biosciences) for 1 h at 25˚C. Antibody antigen complexes were detected using Ultra-sensitive ECL Substrate (cat. no. AR1191; Boster Biological Technology). For the densitometric quantification of the blots, ImageJ software (version 1.8; National Institutes of Health) was used. Each experimental condition was replicated in three separate assays.

Cell viability assay. A Cell-Counting Kit-8 (CCK-8) assay (cat. no. AR1160; Boster Biological Technology) was used to assess cell viability. Cells were seeded in a 96-well plate at a density of 5,000-10,000 cells/well in 100 μl media and incubated at 37˚C for 24 h. After incubation, 10 μl CCK-8 solution was added to each well and the plate was incubated for 1 h. The absorbance at 450 nm was measured using a microplate reader after 24, 48, 72, 96 and 120 h. Three replicate wells were used for each time point, and the mean absorbance value was calculated to plot cell growth curves.

Colony formation assay. To evaluate colony formation, 500-1,000 cells were seeded into 6-well plates and cultured for 2 weeks. Subsequently, the cells were fixed using 4% paraformaldehyde at room temperature for 15-30 min and stained using 0.5% crystal violet at room temperature for 10-20 min. Colonies consisting of >50 cells were considered viable and counted using a light microscope. Each experimental condition was replicated in three separate assays.

Transwell invasion and migration assay. Transwell invasion assays were performed using 24-well Transwell plates with 8-μm pores (Corning Inc.), pre-coated with Matrigel (cat. no. Falcon 354480; BD Biosciences), which were incubated in a 37˚C incubator for 30 min to 1 h until the Matrigel was completely solidified to form a uniform gel layer. A

suspension containing $1x10^5$ cells in 500 μl DMEM with 1% FBS was added to the upper chamber, while 750 μl DMEM supplemented with 10% FBS was added to the lower chamber. After 48 h of incubation, the Matrigel and cells remaining in the upper chamber were removed using cotton swabs. The cells on the lower surface of the membrane were fixed in 4% paraformaldehyde at room temperature for 20-30 min and then stained with 0.5% crystal violet at room temperature for 15-30 min. Subsequently, cells in five microscopic fields (x200 magnification) were counted and images captured. All experiments were conducted in triplicate. For the migration assay, Transwell plates that were not coated with Matrigel were utilized. The remaining steps were similar to those of the invasion assay, with the exception of omitting the Matrigel coating and solidification processes.

Enzyme-linked immunosorbent assay (ELISA). Cells were cultured in a 6-well plate, until the cell count reached ~$1x10^6$, with a cell density of 70-80%. At this point, the culture medium was collected and centrifuged at 1,000 x g for 20 min at 2-8˚C to remove impurities and cell debris, and the supernatant was separated for analysis. The levels of IL-1β and IL-18 in the supernatant were determined using Human IL-1β ELISA Kit (cat. no. SEKH-0002, Beijing Solarbio Science & Technology Co., Ltd.) and Human IL-18 ELISA Kit (cat. no. SEKH-0028), according to the manufacturer's protocol. A linear fit method was used to generate a standard curve. Each experimental condition was replicated in three separate assays.

Flow cytometry. Cells were cultured in a 6-well plate, until a cell count of ~$1x10^6$ and a cell density of 70-80% were achieved. The cells were then collected, processed into a single-cell suspension, and centrifuged at 300 x g for 5 min at 25˚C. Subsequently, the cells were washed twice with 4 ml flow buffer, centrifuged at 300 x g for 5 min at 4˚C, and then resuspended in 0.5 ml flow buffer. After adding 5 μl Annexin V/FITC and mixing well, the mixture was incubated at room temperature in the dark for 5 min. Next, 5 μl propidium iodide (PI) solution and 400 μl PBS were added, and flow cytometry detection was performed. Cell apoptosis was determined using an Annexin V-FITC Apoptosis Detection Kit (cat. no. CA1020; Beijing Solarbio Science & Technology Co., Ltd.). A total of 100 μl cell suspension containing $1x10^6$ cells was taken and 20 μl Fc receptor blocker was added before incubation at room temperature for 5-10 min. Next, 0.625 μl CD86 antibody (cat. no. 12-0862-82; Thermo Fisher Scientific, Inc.) was added to stain the cells, which were incubated on ice in the dark for 30-60 min. Subsequently, 1 ml flow cytometry staining buffer was added to wash the cells, which were then centrifuged at 400-600 x g for 5 min at room temperature. This washing step was repeated before detection. Flow cytometry analysis was performed using a BD FACSCelesta™ flow cytometer (BD Biosciences), and the data were analyzed using FlowJo version 10.8.1 (FlowJo LLC). Each experimental condition was replicated in three separate assays.

Transcriptomics and proteomics sequencing. SiHa cells in which the expression of MIF had been knocked down and the corresponding negative control cells (*vide infra*) were collected during the logarithmic growth. As previously mentioned, total RNA and protein was extracted from the cells. Cells with a transfection efficiency >80% were selected for transcriptomics and proteomics sequencing.

The transcriptome data were generated using the Illumina sequencing platform and the raw data were processed to obtain high-quality clean reads. Total RNA was extracted from cells using Total RNA Extraction Kit (cat. no. R1200; Beijing Solarbio Science & Technology Co., Ltd.). To verify the quality and integrity of the samples, the Agilent 2100 bioanalyzer was used to analyze the RNA Integrity Number for assessing the completeness and purity of the RNA. The sequencing kit used was the NEBNext® Ultra™ RNA Library Prep Kit for Illumina® (NEB #E7530S/L; New England Biolabs). After preparing the sequencing library, its concentration was measured to ensure that the optimal concentration of the library was loaded onto the sequencer. The final loading concentration of the library was 10 nM. The Illumina NovaSeq 6000 (Illumina, Inc.) sequencing instrument was used, employing paired-end sequencing with a nucleotide length of 150 bp. The DESeq2 software package (version 1.20.0; https://bioconductor.org/packages/release/bioc/html/DESeq2.html) was used for inter-sample differential gene analysis. The expression ratios between the two groups of samples were expressed as fold change (FC) values, with screening criteria of $P<0.05$ and $|\log_2 FC|>1$ for differentially expressed genes (DEGs). Statistical analysis was performed with corrections for multiple comparisons using the false discovery rate method.

A 0.2-mg protein sample was used for Tandem Mass Tag analysis, using TMT® Mass Tagging Kits and Reagents according to the manufacturer's protocol (Thermo Fisher Scientific, Inc.). A high-resolution mass spectrometer (Q Exactive™ plus; Thermo Fisher Scientific, Inc.) was used to perform the quantitative proteomics analysis. The mass spectrometer employed a data-dependent acquisition mode, with a full scan range of 350-1,500 m/z. The resulting spectra from each run were searched separately against 1327172-1327172-Homo_sapiens using the Fasta (109,914 sequences) database with the Proteome Discoverer 2.4 search engine (Thermo Fisher Scientific, Inc.). Proteins with significant differences between the two groups of cells ($P<0.05$ and $|\log_2 FC|>1$), were considered differentially expressed proteins. Each experimental condition was replicated in three separate assays.

MIF knockdown. To generate retroviral vectors containing short hairpin RNAs (shRNAs) targeting *MIF* and a shRNA control (shCtrl) the following oligodeoxyribonucleotide sequences were annealed and subcloned between the *Age*I and *Eco*RI restriction sites of a BR-V108 vector (Shanghai GeneChem Co., Ltd.): shCtrl: Pbr17579-a, CCGGGGGCCTCTTTCTGCTCT ATAACTCGAGTTATAGAGCAGAAAGAGGCCCTTTTTG and Pbr17579-b, AATTCAAAAAGGGCCTCTTTCTGCTCT ATAACTCGAGTTATAGAGCAGAAAGAGGCCC; shMIF-1: Pbr17580-a, CCGGGGGTCTACATCAACTATTACTCGAGT AATAGTTGATGTAGACCCTTTTTG and Pbr17580-b, AAT TCAAAAAGGGTCTACATCAACTATTACTCGAGTAAT AGTTGATGTAGACCC; shMIF-2: Pbr17581-a, CCGGTG CCAGTACGTGCAAGGTGTTCTCGAGAACACCTTGCAC GTACTGGCATTTTTG and Pbr17581-b, AATTCAAAAATG

CCAGTACGTGCAAGGTGTTCTCGAGAACACCTTGCA CGTACTGGCA.

Retroviral particles were generated through the transfection of TOP10 *E. coli* Competent cells (cat. no. CB104-03, Tiangen Biotech, Co., Ltd.) with the BR-V108 constructs and the necessary packaging plasmids, using Lipofectamine® 2000 (Thermo Fisher Scientific, Inc.). A second-generation lentiviral packaging system was employed, utilizing 20 μg GV vector plasmid, 15 μg pHelper 1.0 vector plasmid and 10 μg pHelper 2.0 vector plasmid for transfection. The transfection was incubated in a 37˚C incubator for 72-96 h. Regarding the multiplicity of infection, a value of 10 was used to infect the target cells. SiHa and CaSki cells were cultured in 6-well plates until they reached 50-60% confluence. Subsequently, the cells were transduced with either shRNA or the empty BR-V108 vector (negative control) in a 37˚C incubator for 72-96 h and selected in a medium containing 10 μg/ml Puromycin for 3-4 days to allow for the selection of stably transfected cells. The efficiency of *MIF* knockdown was assessed at various time points.

MIF and TSC22D3 overexpression. The pcDNA3 expression plasmids were acquired from Invitrogen (Thermo Fisher Scientific, Inc.). The empty plasmid was employed as a control, with a transfection concentration of 1.5 μg/ml. Plasmid transfection was carried out using Lipofectamine 2000 according to the manufacturer's guidelines. In brief, cells were plated in 6-well plates at a concentration of $2x10^5$ cells/well and permitted to adhere overnight. Subsequently, the plasmid was diluted in Opti-MEM medium (Life Technologies; Thermo Fisher Scientific, Inc.) and combined with Lipofectamine 2000. This combination was then introduced to the cells and incubated for 4-6 h at 37˚C in an atmosphere containing 5% CO_2. The medium was then exchanged with fresh DMEM supplemented with 10% FBS, and the cells were further incubated for 24 h in an environment of 95% air and 5% CO_2 prior to use in subsequent experiments. The empty plasmid served as the control (Ctrl) for MIF-OE and TSC22D3-OE.

To prepare cells with shMIF/TSC22D3-OE co-transfections, the SiHa cells with *MIF* knockdown were combined with the TSC22D3-OE plasmid and Lipofectamine 2000, and subjected to the aforementioned transfection protocol. The efficiency of overexpression or knockdown was assessed at various time points.

Induction and differentiation of THP-1 cells. Following the adjustment of THP-1 cell density to $5x10^5$ cells/ml, 2 ml cell suspension was added to each well of a 6-well plate, and supplemented with phorbol 12-myristate 13-acetate (100 ng/ml). The plate was then incubated in a constant temperature incubator at 37˚C with 5% CO_2 for 48 h. When 85% of the suspended THP-1 monocytes had adhered to the plate, the supernatant was aspirated and discarded, and replenishment with fresh complete medium was performed. Differentiation was induced by adding LPS (100 ng/ml) and IFN-γ (20 ng/ml) for M1 polarization, and IL-4 (20 ng/ml) for M2 polarization. The cells were further incubated in under the same incubator conditions for an additional 48 h. Under high-power microscopy, the cells exhibited larger cell bodies and elongated protrusions, indicating differentiation into M1 and M2 macrophages, respectively. Each experimental condition was replicated in three separate assays.

Bioinformatics. Publicly available databases were used for expression, survival and prognostic analyses. For analysis using the Gene Expression Profiling Interactive Analysis (GEPIA) database (http://gepia.cancer-pku.cn/), the expression of MIF was compared between normal and CSCC tissues, and among different cancer stages. In addition, in the 'Survival Analysis' module, the gene symbol MIF was input, the specific tumor type was selected, and overall survival (OS) was analyzed. It was not possible to restrict the time range in GEPIA to remove the late-stage crossover of the survival curves. Similarly, the UALCAN database (http://ualcan.path.uab.edu/) was used to compare the expression of MIF between normal and primary CSCC tissues, and among different cancer stages. Kaplan-Meier Plotter (http://kmplot.com/analysis/) was used to generate the Kaplan-Meier survival curve.

Statistical analysis. Statistical analysis was performed using SPSS version 22.0 (IBM Corp.). Graphs were created and analyzed using GraphPad Prism version 9.5 (Dotmatics) and Adobe Illustrator Creative Cloud 2017 (Adobe Systems Europe, Ltd.). For quantitative data, normality and homogeneity of variance were assessed. Data with a normal distribution were expressed as the mean ± standard deviation, while non-normally distributed data were presented as the median (interquartile range). When comparing data between two groups, an independent samples t-test was used if the data were normally distributed and a Mann-Whitney U test was used for non-normally distributed data. Comparisons between multiple groups were performed using a one-way ANOVA followed by least significant difference or Tukey's post hoc tests. $P<0.05$ was considered to indicate a statistically significant difference.

Results

MIF is significantly upregulated in CSCC and associated with a poor prognosis. Initial analysis of MIF expression in cervical cancer using the GEPIA database revealed that MIF levels in cervical cancer tissues were significantly elevated compared with those in normal cervical tissues (Fig. 1A). Further analysis using the UALCAN database confirmed that MIF expression in cervical cancer was higher than that in normal tissue (Fig. 1C). Additionally, MIF expression levels increased as the stage of cervical cancer increased, as evidenced by analyses from both databases (Fig. 1B and D). In fresh CSCC tissues, MIF expression levels were significantly higher in the tissues of patients with lymph node metastasis than in those without (Fig. 1E-G). Furthermore, MIF expression levels were significantly elevated in the SiHa and CaSki CSCC cell lines compared with those in the H8 normal cervical epithelial cell line (Fig. 1H), highlighting the potential role of MIF in cervical cancer progression. Analysis of OS data from 292 patients with cervical cancer using GEPIA indicated that high MIF expression was associated with significantly poorer OS compared with that of patients with low MIF expression (Fig. 1I). This was corroborated by data obtained using Kaplan-Meier Plotter, confirming the association between high MIF expression and

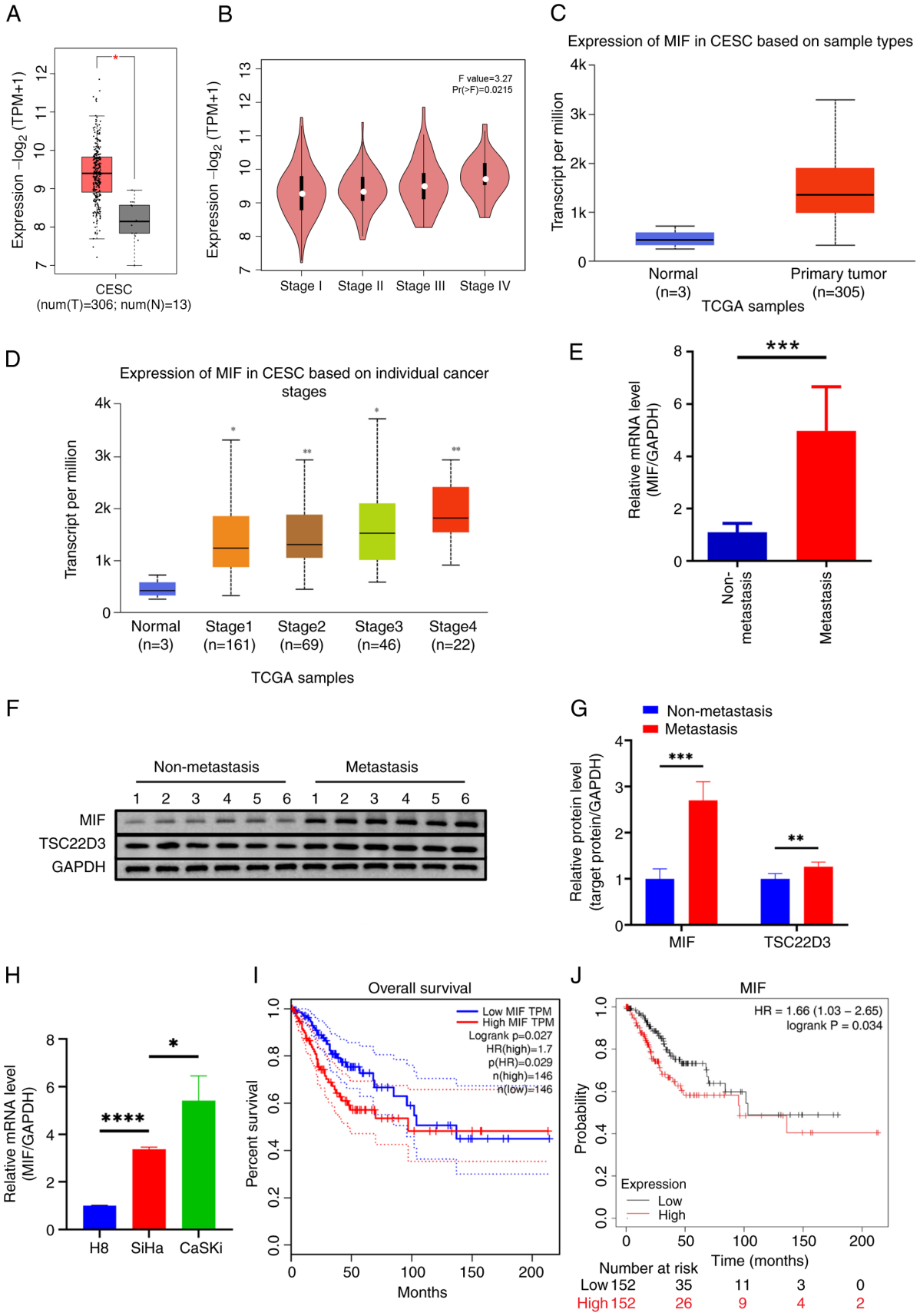

Figure 1. MIF is significantly upregulated in CSCC. MIF is highly expressed in CSCC tissue based on data obtained from the (A) GEPIA and (B) UALCAN databases. MIF expression was positively correlated with CSCC stage according to (C) GEPIA and (D) UALCAN data. (E) RT-qPCR and (F and G) western blotting were used to determine the mRNA and protein expression of MIF in CSCC tissues, respectively. (H) RT-qPCR analysis of the mRNA expression of *MIF* in CSCC and normal cervical cell lines. Data from (I) GEPIA and (J) Kaplan-Meier Plotter showed that the overall survival of patients with highly MIF expressing cervical cancer was poor. *P<0.05, **P<0.01, ***P<0.001, ****P<0.0001. MIF, macrophage migration inhibitory factor; CSCC/CESC, cervical squamous cell carcinoma; T, tumor tissue; N, normal tissue; TPM, transcripts per million; Pr(>F), P-value of the F statistic; TCGA, The Cancer Genome Atlas; RT-qPCR, reverse transcription-quantitative polymerase chain reaction; TSC22D3, TSC22 domain family protein 3; HR, hazard ratio.

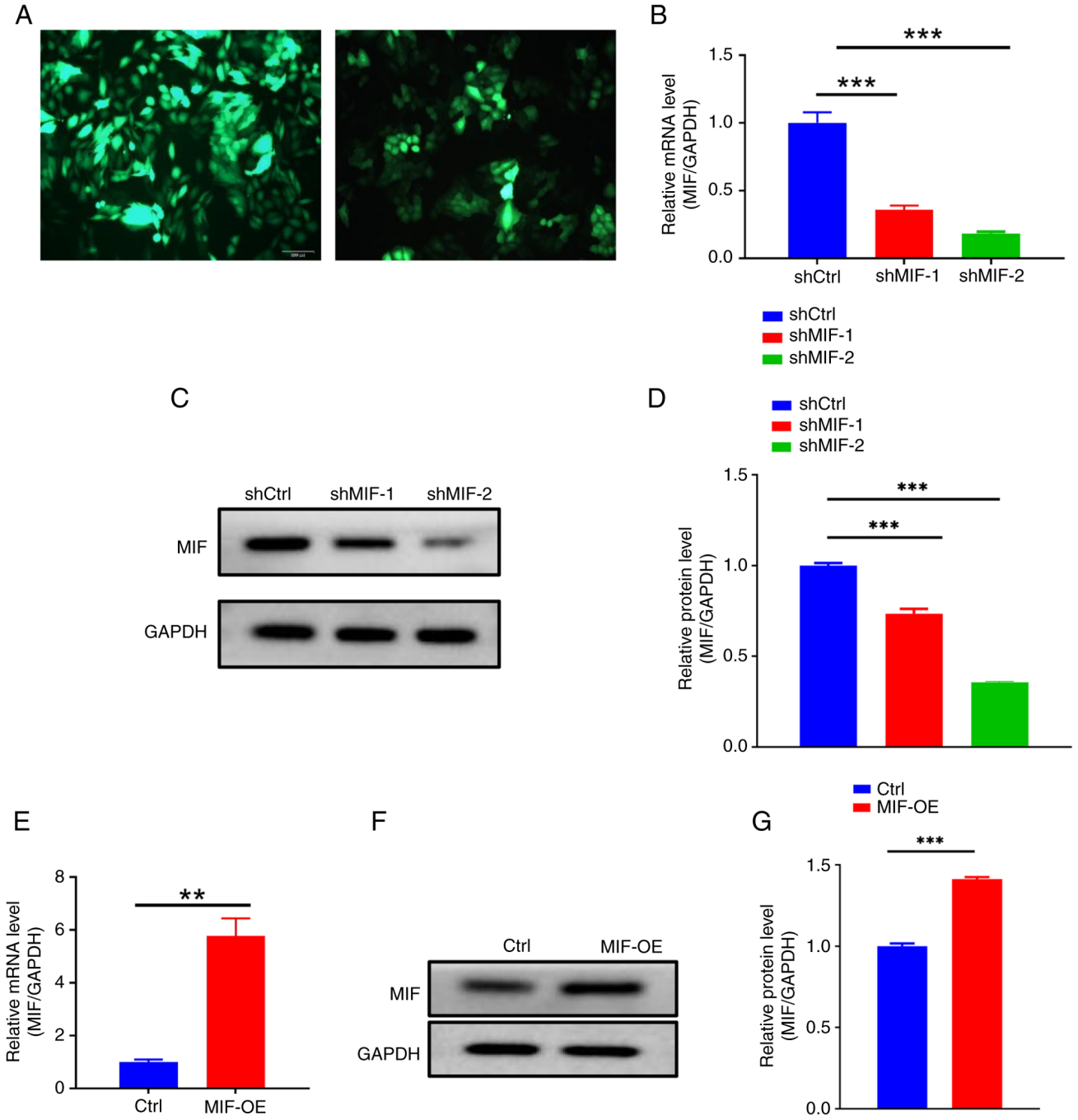

Figure 2. Verification of *MIF* knockdown and overexpression. (A) Fluorescence efficiency in *MIF* knockdown lentivirus-infected SiHa and CaSki cells; left panel, SiHa; right panel, CaSki. Magnification, x200. (B) RT-qPCR was used to determine the efficiency of *MIF* knockdown. (C and D) Western blotting was used to confirm that the protein expression of MIF was also reduced. (E) RT-qPCR was used to verify *MIF* overexpression in the transfected cells. (F and G) western blotting confirmed MIF overexpression at the protein level. **P<0.01, ***P<0.001. MIF, macrophage migration inhibitory factor; RT-qPCR, reverse transcription-quantitative polymerase chain reaction; shMIF, short-hairpin RNA targeting MIF; shCtrl, short-hairpin RNA control; OE, overexpression; Ctrl, empty vector control.

reduced OS in patients with cervical cancer (Fig. 1J). These results underscore the potential significance of MIF in cervical cancer progression and prognosis.

MIF promotes CSCC progression and is associated with inflammasome activation. To investigate the impact of MIF on the malignant behavior of CSCC, *MIF*-knockdown plasmids were designed and packaged into lentiviral particles for transfection into SiHa and CaSki CSCC cells. Fluorescence microscopy revealed markedly higher fluorescence intensity in the SiHa cells than in the CaSki cells (Fig. 2A), indicating superior infection efficiency in the SiHa cells. Therefore, SiHa cells were selected for use in subsequent experiments. The efficiency of *MIF* knockdown and overexpression in the SiHa cells was then evaluated (Fig. 2B-G).

To investigate the effects of *MIF* knockdown on CSCC progression, a CCK-8 assay was performed, which revealed a significant reduction in the proliferative ability of SiHa cells

in the shMIF groups compared with that of cells in the control group (Fig. 3A). Additionally, flow cytometry indicated a notable increase in the total percentage of apoptotic SiHa cells in the shMIF groups compared with that in the control group, with significantly higher percentages of both early and late apoptotic cells (Fig. 3D). The colony formation assay demonstrated a substantial reduction in the colony formation capacity of SiHa cells in the shMIF groups, as evidenced by a significant reduction in the number of colonies compared with those in the control group, as well as a clear reduction in the area of the colonies (Fig. 3E). Furthermore, the Transwell assay revealed a significant reduction in the invasive capacity of SiHa cells in the shMIF groups compared with that of the control group (Fig. 3F).

Further investigation of changes in the inflammasome following *MIF* knockdown included assessment of the expression of the inflammasome-related proteins NLRP3, ASC and caspase-1 and their respective mRNAs. The results revealed significant reductions in the mRNA and protein expression levels of NLRP3, ASC and caspase-1 in the shMIF groups compared with those in the control group (Fig. 3G-J). Additionally, the ELISA analysis of inflammasome-related factors IL-1β and IL-18 in the supernatant of SiHa cells revealed that secretion of these factors was reduced following *MIF* knockdown compared with that in the control group (Fig. 3B and C).

By comparison, the proliferative ability of cells in the MIF-OE group was significantly higher than that of cells in the control group (Fig. 4A). In addition, flow cytometry revealed a significant reduction in the apoptotic rate of the MIF-OE group compared with that of the control (Fig. 4D). Additionally, the colony formation assay showed a significant increase in the colony formation capacity of the cells due to *MIF* overexpression (Fig. 4E). The results of the Transwell assays indicated a significant increase in the invasive ability of cells following *MIF* overexpression (Fig. 4F). The expression of inflammasome-related proteins and their respective mRNAs was assessed, and significant increases for all proteins and mRNAs were observed in the MIF-OE group compared with those in the control group (Fig. 4G and H). Furthermore, ELISA analysis revealed that *MIF* overexpression significantly increased the levels of IL-1β and IL-18 in the supernatant of SiHa cells (Fig. 4B and C). These results suggest that MIF may promote CSCC progression and is associated with inflammasome activation.

TSC22D3 is a key MIF-interacting gene based on multi-omics screening. To investigate downstream molecules potentially regulated by MIF in the development of CSCC, SiHa cells with the knockdown of *MIF* expression were used for transcriptomic and proteomic sequencing to identify changes in the expression of the downstream genes, both upregulated and downregulated. Based on the observation that shMIF-2 exhibits higher knockdown efficiency than shMIF-1, shMIF-2 was selected for use in subsequent experiments. DEGs were screened based on criteria of $P<0.05$ and $|\log_2 FC|>1$. Heat maps and volcano plots were generated following the multi-omics screening of downstream genes (Figs. 5, 6A and B). Correlation analysis of the multi-omics sequencing results revealed 10 common DEGs in both the transcriptome and proteome sequencing data ($P<0.005$ and $|\log 2FC|>0.5$; Fig. 6C), consisting of three upregulated genes (*PSCA* and *LAMB1*) and eight downregulated genes (*SLC35F2*, *SLC1A4*, *ACAP3*, *OSBPL6*, *TSC22D3*, *ASNS*, *F3* and *TRIB3)*. Validation performed by the RT-qPCR analysis of *MIF*-knockdown SiHa cells confirmed the significant upregulation of *PSCA* and *LAMB1* ($P<0.01$) and significant downregulation of *SLC35F2*, *SLC14A*, *ACAP3*, *OSBPL6*, *TSC22D3*, *ASNS*, *F3* and *TRIB3* ($P<0.05$; Fig. 6D). The experimental validation of MIF expression aligned with the results of sequencing, confirming the reliability of these results. The downregulated gene *TSC22D3* was selected for further investigation given the limited reports on its role in cervical cancer. Notably, its known roles in inflammation and immune regulation suggest a significant role in the regulation of tumor growth (17-20); therefore, it is hypothesized that TSC22D3 may significantly influence CSCC progression.

Subsequently, the expression of *TSC22D3* in CSCC tissues was investigated. The findings revealed that the mRNA and protein expression levels of TSC22D3 in the tissues of patients with lymph node metastasis were significantly higher compared with those in the tissues of patients without lymph node metastasis (Figs. 1F and G, and 6E). These results suggest that *TSC22D3* may be a pivotal gene with similar pro-tumor inflammatory properties to MIF, and their combined interaction may promote CSCC progression.

Interaction between MIF and TSC22D3 regulates inflammasome activation in CSCC progression. Rescue experiments were performed to explore the functional interaction between MIF and TSC22D3. Separate *MIF* knockdown and *TSC22D3* overexpression plasmids were constructed and packaged into lentiviruses, which were co-infected into SiHa cells. The transfection efficiency of the plasmids was subsequently confirmed (Fig. 7A-B, D-E).

Experiments were then performed to investigate the biological behaviors of the transfected SiHa cells. The results of the CCK-8 assays indicate a significant reduction in the proliferative capacity of SiHa cells in the shMIF group compared with the control group (Fig. 7C). Moreover, following *TSC22D3* overexpression, the proliferative ability of SiHa cells in the shMIF + OE-TSC22D3 group was higher than that in the shMIF group, yet lower than that in the OE-TSC22D3 group, although this latter variation has not yet shown statistical differences. These findings suggest that *TSC22D3* overexpression may partially reversed the reduction in proliferation of SiHa cells induced by *MIF* knockdown. Moreover, the analysis of apoptosis using flow cytometry indicated that *TSC22D3* overexpression partially attenuated the increase in apoptosis of SiHa cells following *MIF* knockdown (Fig. 7F and I). In addition, colony formation assays demonstrated that *TSC22D3* overexpression partially reversed the reduction in the colony formation capacity of SiHa cells following *MIF* knockdown (Fig. 7G and H). The results of the Transwell invasion assays are presented in Fig. 7J and K, and indicate that the number of invasive SiHa cells in the shMIF group was significantly reduced compared with that in the control group. This suggests that the knockdown of MIF had an inhibitory effect on the invasive capacity of SiHa cells. Furthermore, the overexpression of TSC22D3 in the shMIF + OE-TSC22D3 group resulted in a partial restoration of the invasive ability of SiHa cells, as evidenced by an increase in the number of invasive cells

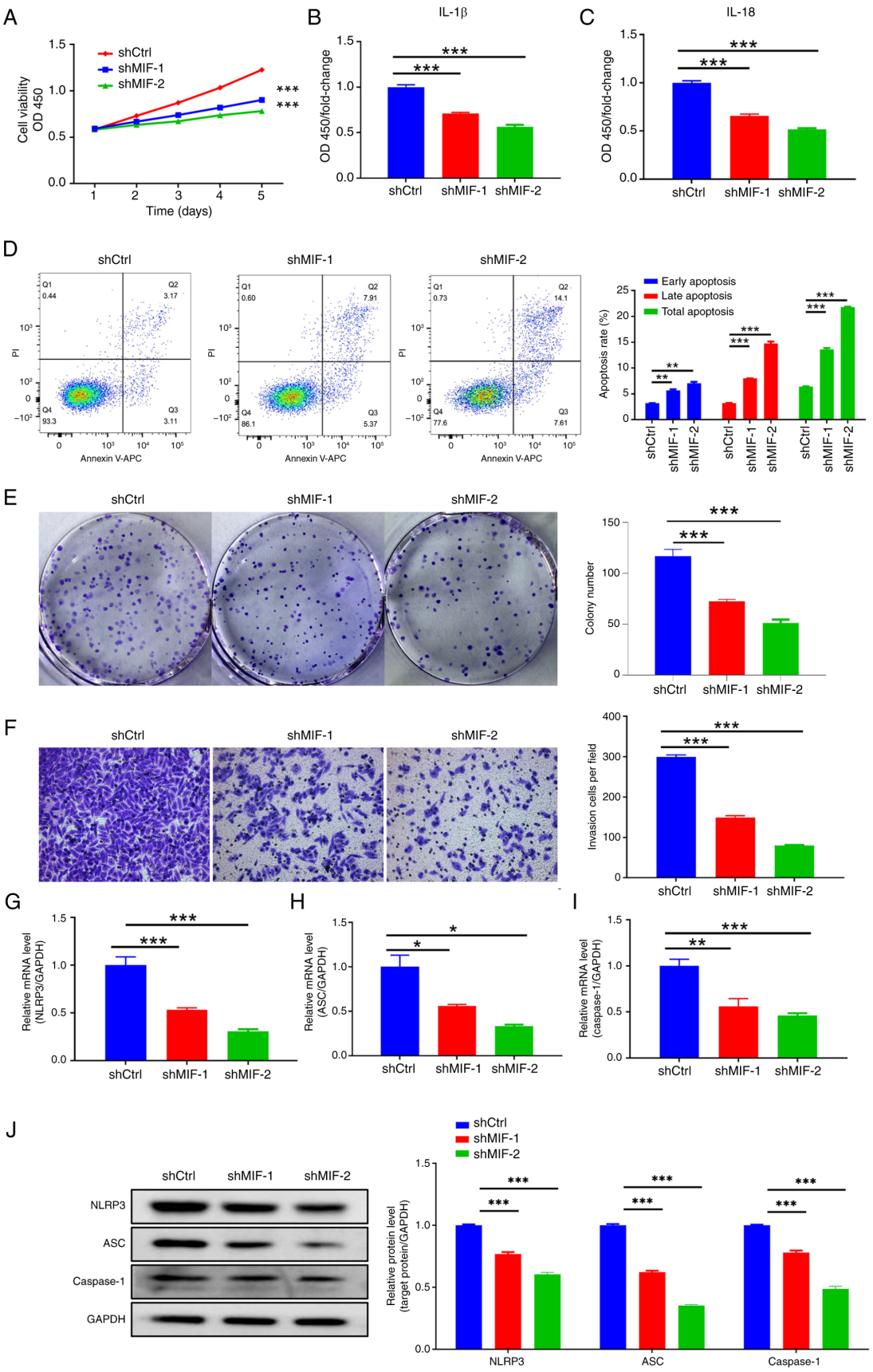

Figure 3. *MIF* knockdown inhibits cervical squamous cell carcinoma progression. (A) Cell Counting Kit-8 showing the proliferation of SiHa cells following MIF knockdown. Enzyme-linked immunosorbent assays showing the expression of the inflammasome-associated proteins (B) IL-1β and (C) IL-18 following MIF knockdown. (D) Flow cytometry, (E) colony formation and (F) Transwell invasion assays (magnification, x200) showing the apoptosis and invasion of SiHa cells following MIF knockdown. (G-I) Reverse transcription-quantitative polymerase chain reaction and (J) western blotting assays were used to determine the expression of the inflammasome-associated mRNA and proteins NLRP3, ASC and caspase-1 following MIF knockdown. *P<0.05, **P<0.01, ***P<0.001 vs. shCtrl. MIF, macrophage migration inhibitory factor; OD, optical density; OD450, OD at 450 nm; shCtrl, short-hairpin RNA control; shMIF, short-hairpin RNA targeting MIF; NLRP3, NLR family pyrin domain containing 3; ASC, apoptosis-associated speck-like protein containing a CARD.

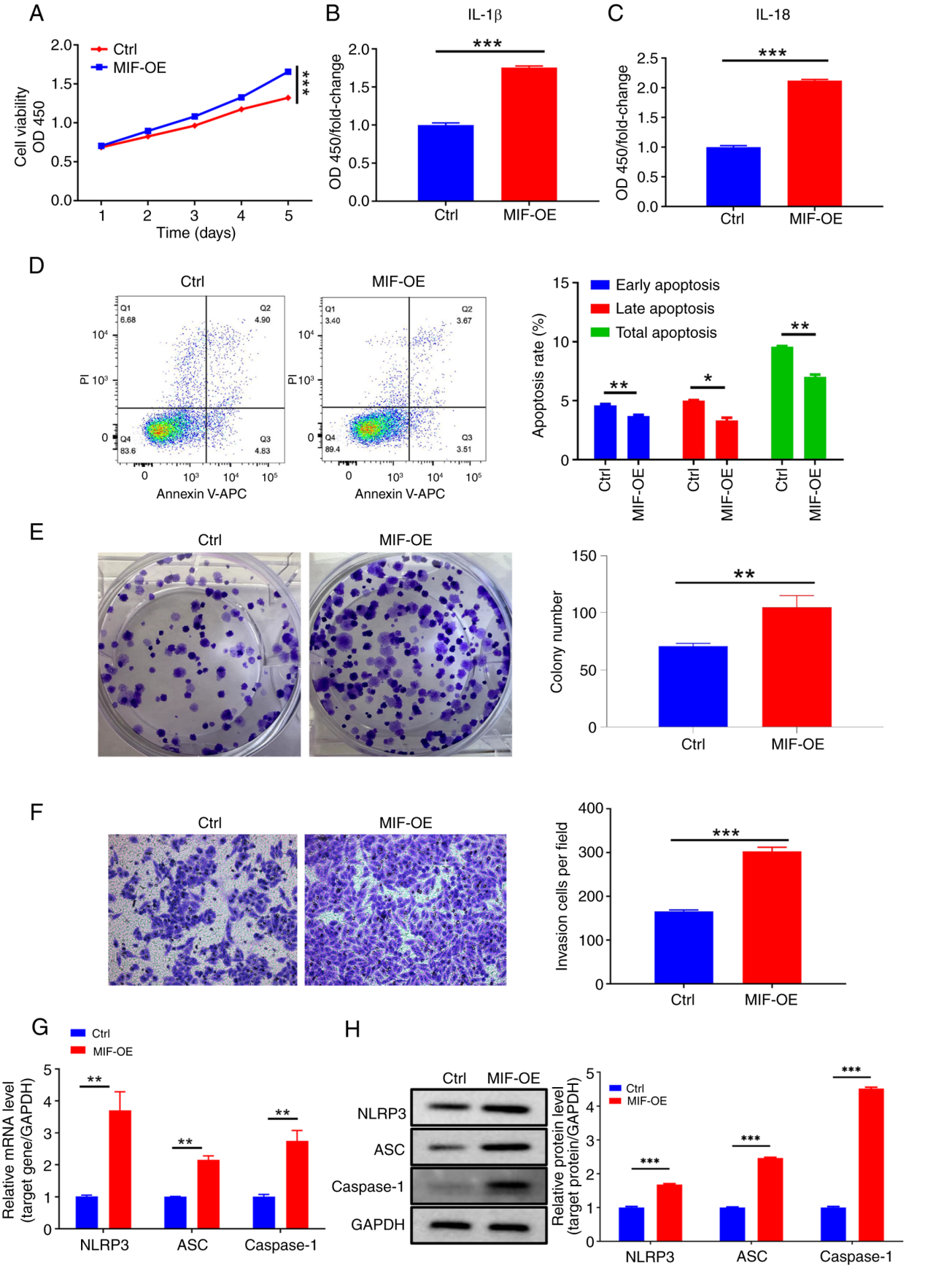

Figure 4. *MIF* overexpression promotes cervical squamous cell carcinoma cell growth and invasive behavior. (A) Cell Counting Kit-8 analysis of SiHa cells following MIF overexpression. (B and C) Enzyme-linked immunosorbent assays showing the expression of inflammasome proteins IL-1β and IL-18 following MIF overexpression. (D) Flow cytometry, (E) colony formation and (F) Transwell invasion assays (magnification, x200) of SiHa cells following MIF overexpression. (G) Reverse transcription-quantitative polymerase chain reaction and (H) western blot analyses of the mRNA and protein expression levels of the inflammasome-related mRNAs and proteins NLRP3, ASC and caspase-1 following MIF overexpression. *P<0.05, **P<0.01, ***P<0.001. MIF, macrophage migration inhibitory factor; OD450, optical density at 450 nm; OE, overexpression vector; Ctrl, empty vector control; IL, interleukin.

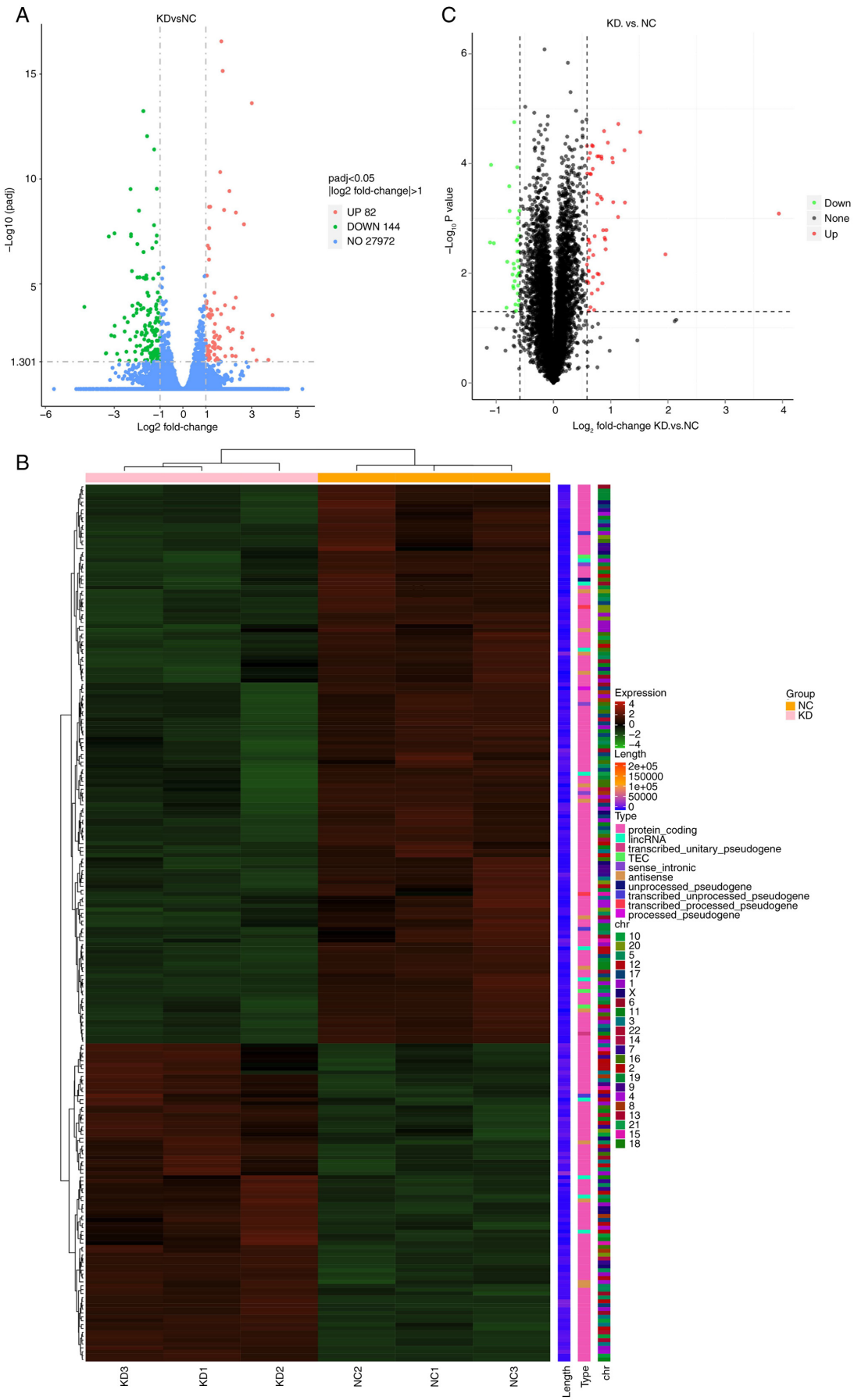

Figure 5. Screening of downstream genes potentially regulated by MIF and TSC22D3. (A) Volcano plot and (B) heatmap of clustered differentially expressed genes in the transcriptome after *MIF* knockdown. (C) Volcano plot of expressed proteins in the proteome following MIF knockdown. Red represents high expression and green represents low expression. MIF, macrophage migration inhibitory factor; TSC22D3, TSC22 domain family protein 3; KD, knockdown of MIF; NC, negative control; padj, adjusted P-value; lincRNA, long intergenic non-coding RNA; TEC, to be experimentally confirmed; chr, chromosome.

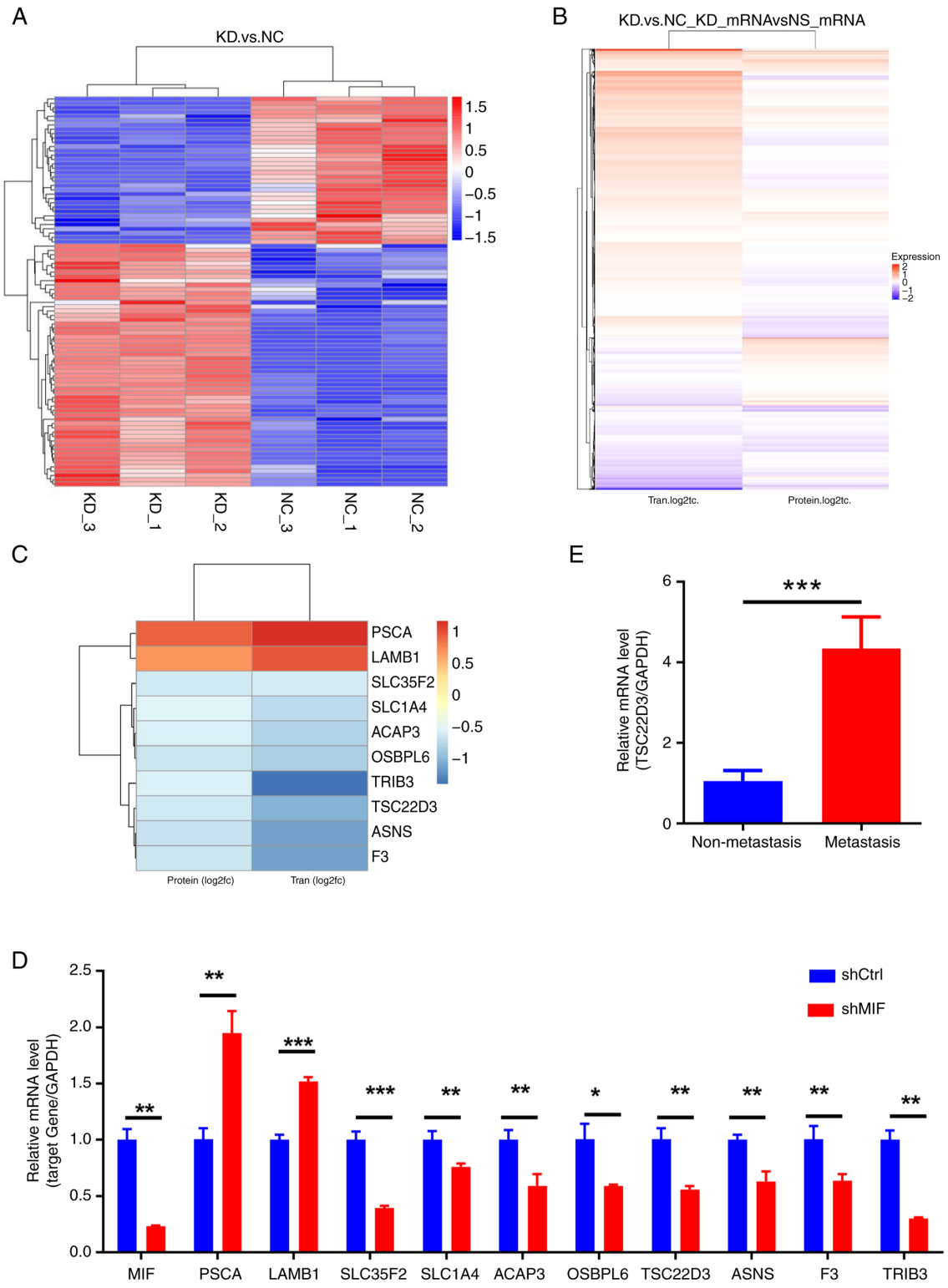

Figure 6. Multi-omics screening of downstream genes potentially regulated by MIF and TSC22D3. (A) Heatmap of clustered differentially expressed proteins in the proteome following *MIF* knockdown. (B) Heatmap of the correlation between transcriptome and proteome expression levels. (C) Heatmap of clustered genes common to both the transcriptome and proteome. (D) RT-qPCR validation of candidate genes identified through multi-omics screening. (E) RT-qPCR detection of *TSC22D3* in cervical squamous cell carcinoma tissues. *P<0.05, **P<0.01, ***P<0.001. MIF, macrophage migration inhibitory factor; TSC22D3, TSC22 domain family protein 3; RT-qPCR, reverse transcription-quantitative polymerase chain reaction; KD, knockdown of MIF; NC, negative control; Tran, transcript; PSCA, prostate stem cell antigen; LAMB1, laminin subunit b 1; SLC39A10, solute carrier 39 member 10; SLC35F2, solute carrier 35 member F2; SLC1A4, solute carrier family 1 member 4; ACAP3, ArfGAP with coiled-coil, ankyrin repeat and PH domain-containing protein 3; OSBPL6, oxysterol binding protein like 6; ASNS, asparagine synthetase; F3, coagulation factor III; TRIB3, tribbles pseudokinase 3; shCtrl, short-hairpin RNA control; shMIF, short-hairpin RNA targeting MIF.

compared with that in the shMIF group. However, the invasive capacity of the shMIF + OE-TSC22D3 group remained lower than that of the OE-TSC22D3 group, indicating that the overexpression of TSC22D3 can partially reverse these effects.

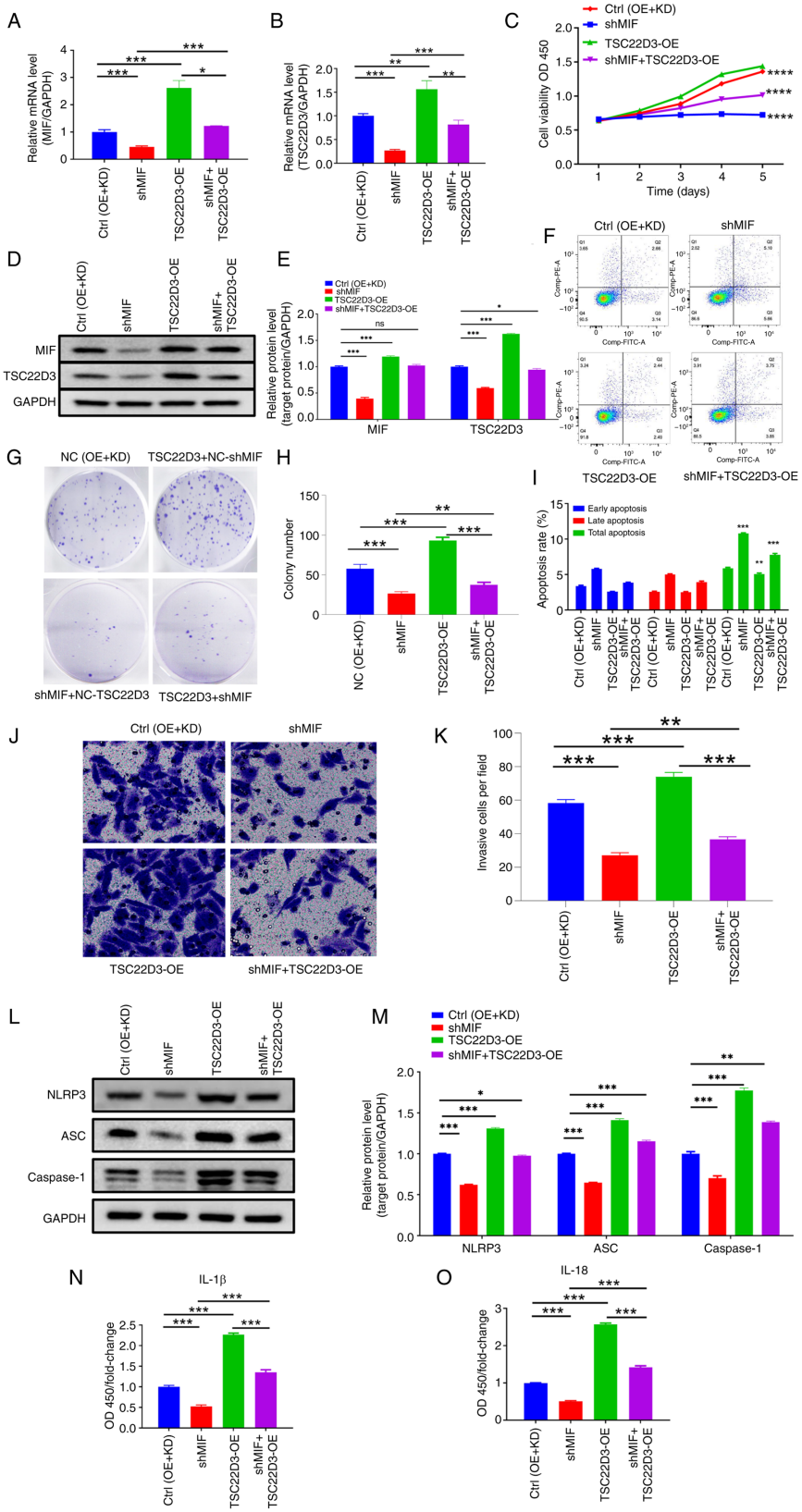

Figure 7. Functional interaction between MIF and TSC22D3 regulates inflammasome activation and cervical squamous cell carcinoma progression. Levels of (A) MIF and (B) TSC22D3 mRNA determined by reverse transcription-quantitative polymerase chain reaction following MIF knockdown and TSC22D3 overexpression. (C) Cell Counting Kit-8 analysis of SiHa cells following MIF knockdown and TSC22D3 overexpression. (D and E) Western blot analysis of MIF and TSC22D3 proteins following MIF knockdown and TSC22D3 overexpression. (F) Flow cytometry and (G) colony formation of SiHa cells following MIF knockdown and TSC22D3 overexpression. Statistical graphs of (H) colony formation and (I) flow cytometry of SiHa cells following MIF knockdown and TSC22D3 overexpression. (J and K) Transwell assays (magnification, x200) of SiHa cells following MIF knockdown and TSC22D3 overexpression. (L-O) Expression of inflammasome-related proteins in SiHa cells following MIF knockdown and TSC22D3 overexpression. (L) Representative western blots and (M) western blot quantification; enzyme-linked immunosorbent assay results for (N) IL-1 and (O) IL-18. *P<0.05, **P<0.01, ***P<0.001, ****P<0.0001. MIF, macrophage migration inhibitory factor; TSC22D3, TSC22 domain family protein 3; Ctrl, empty vector control; OE, overexpression; KD, knockdown; NC, negative control; shMIF, short-hairpin RNA targeting MIF; OD, optical density; OD450, OD at 450 nm; IL, interleukin; ns, not significant.

To investigate the roles of MIF and TSC22D3 in inflammasome formation in CSCC, the expression of inflammasome-related proteins was assessed. The results of western blot analysis revealed that the expression levels of NLRP3, ASC and caspase-1 were significantly reduced in the shMIF group compared with those in the control group. However, upon *TSC22D3* overexpression, the protein expression levels of these inflammasome-related molecules in the shMIF + OE-TSC22D3 group were increased compared with those in the shMIF group, yet were lower than those in the OE-TSC22D3 group (Fig. 7L and M), although this latter variation has not yet shown statistical differences. Furthermore, the results of ELISA analysis indicated that the levels of IL-18 and IL-1β in the supernatant of SiHa cells were significantly decreased in the shMIF group compared with those in the control group. Following *TSC22D3* overexpression, the expression of IL-18 and IL-1β in the supernatant was significantly higher in the shMIF + OE-TSC22D3 group compared with that in the shMIF group, yet significantly lower than that in the OE-TSC22D3 group (Fig. 7N and O). These results indicate that *TSC22D3* overexpression partially reversed the impaired ability of SiHa cells to form inflammasomes following *MIF* knockdown.

Interaction between MIF and TSC22D3 promotes macrophage recruitment and polarization in CSCC. The tumor microenvironment significantly influences cancer initiation and progression, with immune cell infiltration being a crucial target in cancer immunotherapeutic strategies (21-23). Tumor cells release cytokines and other mediators that recruit macrophages and other inflammatory cells, which promote tumor growth and metastasis (24-26). Therefore, the role of MIF, an inflammatory factor, in macrophage recruitment in CSCC was investigated. Supernatants from cultured SiHa cells with established MIF-OE transfection and control cells were collected, and elevated mRNA and protein levels of MIF in the supernatants were confirmed by RT-qPCR and western blotting (Fig. 8A-C). These cell supernatants were then co-cultured with THP-1 cells. Results from the CCK-8 assay demonstrated a significant increase in THP-1 cell proliferation in the MIF-OE group compared with that in the control group (Fig. 8D). Furthermore, co-culture with the MIF-OE-transfected cell supernatant was revealed to induce a significant increase in the number of THP-1 cells migrating across the Transwell membrane compared with that of the control, which is indicative of increased migratory ability post-*MIF* overexpression (Fig. 8E). These findings suggest that the overexpression of *MIF* in CSCC cells may promote macrophage recruitment.

To explore whether MIF regulates macrophage recruitment through its interaction with TSC22D3, *MIF* expression was knocked down and *TSC22D3* expression was overexpressed simultaneously in SiHa cells (Fig. 8F and G). Co-culture of THP-1 cells with the cell culture supernatant caused a significant reduction in the proliferative ability of the cells in the shMIF group compared with that in the control group. Upon *TSC22D3* overexpression, the proliferative ability of THP-1 cells in the shMIF + OE-TSC22D3 group was increased compared with that in the shMIF group, but lower than that in the OE-TSC22D3 group (Fig. 8H), and both comparisons showed statistically significant differences.. This result indicates that *TSC22D3* overexpression partially reversed the reduction in THP-1 cell proliferation caused by *MIF* knockdown. Similarly, Transwell experiments demonstrated that the overexpression of *TSC22D3* significantly attenuated the reduction in the migratory ability of the THP-1 cells following *MIF* knockdown (Fig. 8I).

Macrophages play a pivotal role in the infiltration of inflammatory cells at tumor sites, exhibiting significant functional plasticity and the ability to rapidly polarize between M1 and M2 activation states (27-29). To investigate the role of MIF in the induction of macrophage polarization, *MIF* expression in CSCC SiHa cells was manipulated and the supernatant was cultured with THP-1 cells, which had been induced to undergo polarization towards M1 and M2 macrophage phenotypes. Prior to *MIF* manipulation, RT-qPCR analysis confirmed the successful establishment of the *in vitro* macrophage polarization model by demonstrating the significant upregulation of M1-related genes (*iNOS* and *CD86*) in the M1 control group and M2-related genes (*ARG1* and *CD206*) in the M2 control group (Fig. 9A-D). The subsequent manipulation of *MIF* expression levels in SiHa cells revealed that its overexpression significantly increased the expression levels of the M2 surface markers *ARG1* and *CD206* and decreased the expression levels of the M1 surface markers *iNOS* and *CD86* in the respective macrophage models compared with those in the control group when cultured with the SiHa cell supernatant, whereas *MIF* knockdown yielded the opposite effects (Fig. 9E-L). Flow cytometry corroborated these findings, indicating that *MIF* overexpression significantly increased the expression of the M2 surface marker CD206 and decreased that of the M1 surface marker CD86 compared with that in the control group, whereas *MIF* knockdown induced the opposite effects, with all differences being statistically significant (Fig. 9M-O). These results indicate that *MIF* overexpression promotes macrophage polarization toward the M2 phenotype while inhibiting polarization toward the M1 phenotype.

Discussion

MIF plays a direct role in the regulation of tumor cell biology and indirectly contributes to tumor progression by influencing inflammation, immune responses and remodeling of the tumor microenvironment (30-34). Consequently, MIF is increasingly recognized as a promising target for antitumor drug development. Therefore, it is crucial to comprehensively understand the expression patterns of MIF in tumors and elucidate its regulatory mechanisms in inflammation-related tumor progression. The results of the present study align with those of a previous study (34), with the upregulated expression of MIF in CSCC exhibiting a positive association with cancer progression. Given the pivotal role of tumor-related inflammation in cancer, clarifying the tumorigenic function of MIF in the inflammatory process may offer valuable insights for the development of strategies to inhibit cervical cancer progression. MIF has been reported to be a secreted protein, and can be detected in the supernatant of SiHa cells (32). It is hypothesized that manipulation of the

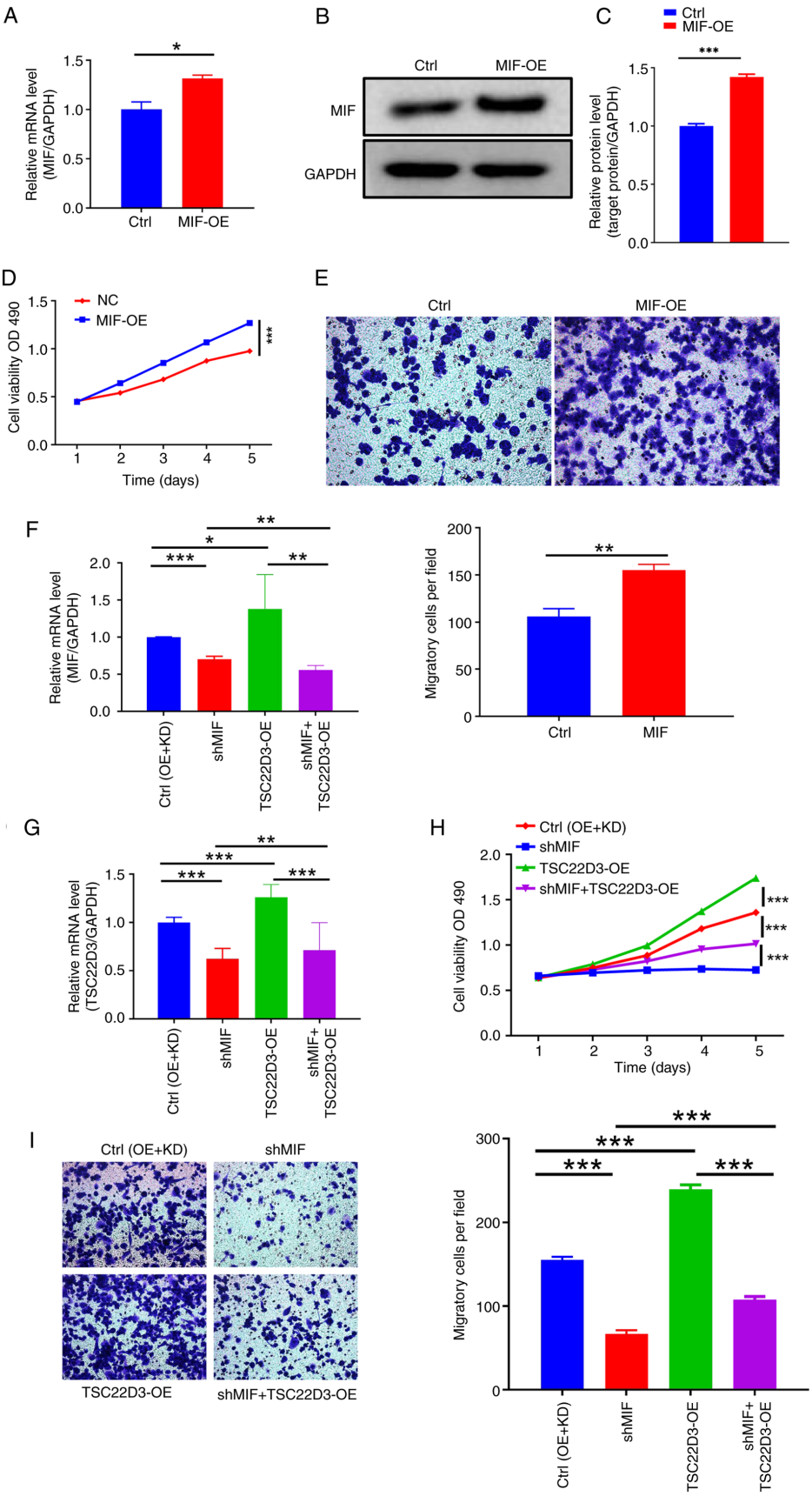

Figure 8. MIF and TSC22D3 interaction in cervical squamous cell carcinoma cells promotes macrophage recruitment. (A-C) Detection of the upregulation of MIF levels in the supernatant of SiHa cells following transfection with *MIF* overexpression vector. MIF levels were assessed by (A) RT-qPCR and (B and C) western blotting. (D) CCK-8 and (E) Transwell assays (magnification, x200) of THP-1 cells following culture with the SiHa cell supernatants. RT-qPCR analysis of the levels of (F) *MIF* and (G) *TSC22D3* in the cell supernatant following *MIF* knockdown and *TSC22D3* overexpression in SiHa cells. (H) CCK-8 and (I) Transwell assays (magnification, x200) of THP-1 cells following culture with the SiHa cell supernatants. *P<0.05, **P<0.01, ***P<0.001. MIF, macrophage migration inhibitory factor; TSC22D3, TSC22 domain family protein 3; RT-qPCR, reverse transcription-quantitative polymerase chain reaction; CCK-8, Cell Counting Kit-8; Ctrl, empty vector control; OE, overexpression; OD, optical density; KD, knockdown; shMIF, short-hairpin RNA targeting MIF.

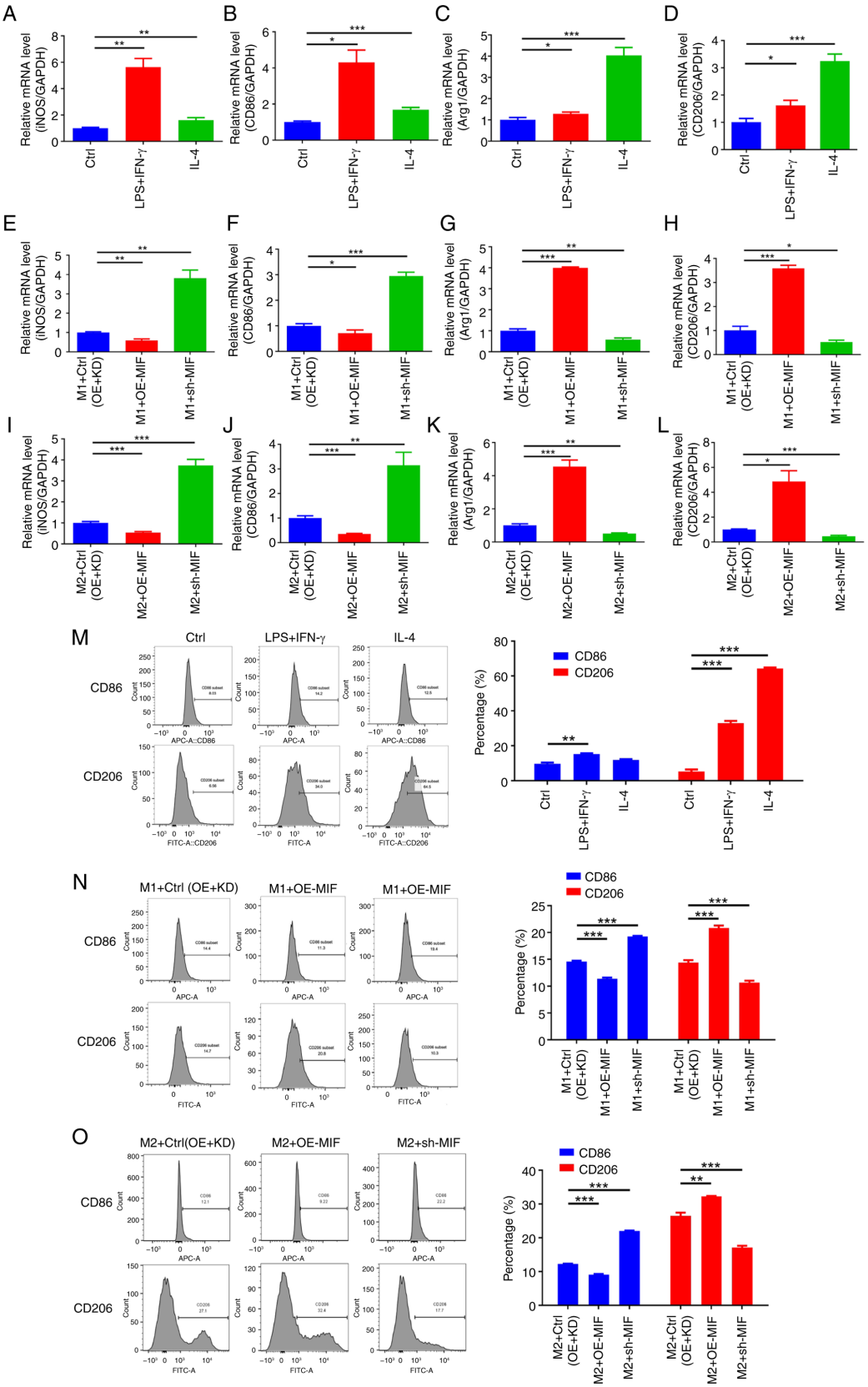

Figure 9. MIF in cervical squamous cell carcinoma cells promotes M2 macrophage polarization. (A-D) RT-qPCR detection of M1 and M2 biomarker expression in THP-1 cells cultured with the supernatant of untransfected SiHa cells. The M1 biomarkers are (A) iNOS and (B) CD86, and M2 biomarkers are (C) Arg1 and (D) CD206. (E-L) RT-qPCR detection of the expression of M1 and M2 biomarkers in THP-1 cells cultured with the supernatants of SiHa cells with manipulated *MIF* levels. (E) *iNOS*, (F) *CD86*, (G) *Arg1* and (H) *CD206* expression in M1-polarized THP-1 cells and (I) *iNOS*, (J) *CD86*, (K) Arg1 and (L) CD206 in M2-polarized THP-1 cells. (M) Flow cytometry analysis of M1/M2 markers in THP-1 cells cultured with untransfected SiHa cell supernatant. Detection of M1/M2 biomarkers in (N) M1- and (O) M2-polarized THP-1 cells following culture with the supernatants of SiHa cells with manipulated *MIF* levels by flow cytometry. *P<0.05, **P<0.01, ***P<0.001. MIF, macrophage migration inhibitory factor; RT-qPCR, reverse transcription-quantitative polymerase chain reaction; iNOS, inducible nitric oxide synthase; Arg1, arginase 1; Ctrl, control; LPS, lipopolysaccharide; IFN, interferon; IL, interleukin; OE, overexpression; KD, knockdown; sh-MIF, short-hairpin RNA targeting MIF.

expression of MIF may affect the expression, secretion or activity of other proteins, such as TSC22D3. This may then influence the secretion or activity of additional proteins, such as the inflammatory factors IL-18 and IL-1β, which could lead to functional changes in neighboring or distant cells, such as macrophages.

The activation of inflammasomes and the resulting cytokine imbalance triggered by pathogen- or damage-associated molecular patterns is a crucial feature in the accelerated progression of inflammation-related tumors (11,35,36). The abnormal activation of NLRP3 sustains chronic inflammation and thus plays a pivotal role in the secretion of pro-inflammatory cytokines during tumor development (37,38). Consequently, the positive association found between MIF expression and the inflammasome-associated molecules NLRP3, ASC, caspase-1, IL-18 and IL-1β in the present study suggest that MIF potentially contributes to CSCC progression via the activation of inflammasome formation, in agreement with a previous study (39).

Transcriptomic and proteomic sequencing were performed in the present study, which identified TSC22D3 as a crucial downstream factor closely associated with the inflammatory tumorigenic function of MIF. Although there is currently limited research on TSC22D3 in CSCC, rescue experiments conducted in this study provided insights suggesting that TSC22D3, in conjunction with MIF, may play a role in certain biological processes related to the development of CSCC and promote the activation of inflammasomes.

The tumor microenvironment plays a crucial role in cancer progression and treatment outcomes. M2 macrophages secrete various growth factors and cytokines, such as vascular endothelial growth factor, platelet-derived growth factor and insulin-like growth factor, which promote tumor cell proliferation, survival and angiogenesis (39). In addition, M2 macrophages inhibit the function of other immune cells, such as T cells and NK cells, thus participating in immunosuppressive responses (40). As MIF is a secreted protein, it can be found in the supernatant of cells that express it. Therefore, it was hypothesized that changes in the expression levels of MIF and TSC22D3 may affect the secretion or activity of other proteins, including inflammatory factors such as IL-18 and IL-1β in the supernatant, which in turn may affect the behavior of neighboring or distant macrophages. Within this context, it was found that MIF and its interacting protein TSC22D3 promoted macrophage migration, and that MIF promoted the transformation of macrophages from an M1 to M2 phenotype. This indicates that MIF could potentially promote cervical cancer progression. It has previously been shown that MIF, via CD74 signaling, exhibits immunosuppressive properties in genitourinary cancer (34). In addition, a study of malignant melanoma demonstrated that CD74-MIF interactions are disrupted by the binding of C36L1 peptide fragment to CD74, which enables macrophages to transform from the M2 to the M1 phenotype, ultimately reactivating cytotoxic T cells (41). However, future efforts are required to substantiate and confirm this mechanism.

The present study has certain limitations. In-depth mechanistic studies using animal models are necessary to understand how MIF and TSC22D3 affect immune cell function and differentiation within the tumor microenvironment. Clinical studies including a larger cohort of patients with CSCC are also required to validate the prognostic value of MIF expression. In addition, investigating the efficacy of targeting MIF in preclinical models and clinical trials could provide valuable insights into its potential as a therapeutic strategy. Further studies should aim to elucidate the specific molecular pathways by which MIF and TSC22D3 influence inflammasome activation and macrophage polarization in the tumor microenvironment. Exploring the crosstalk between MIF-driven inflammation and other signaling pathways implicated in cervical cancer progression may uncover novel therapeutic opportunities. Moreover, investigating the impact of MIF on broader immune responses is essential for gaining a deeper understanding of its overall role in tumor immunity.

In conclusion, the results of the present study provide evidence to suggest that MIF and TSC22D3 have the potential to induce macrophage infiltration in cervical cancer lesions and influence the CSCC tumor microenvironment by polarizing macrophages towards an M2 phenotype, thereby promoting CSCC progression. The present study elucidated the previously unexplored role of MIF in the progression of CSCC *in vitro*, particularly in the context of activation of the inflammasome and modulation of the tumor microenvironment. These findings highlight the potential of targeting the MIF-TSC22D3 axis as a novel therapeutic strategy, offering a promising avenue for improving the efficacy of immunotherapy in the treatment of recurrent or metastatic cervical cancer.

Acknowledgements

The Medical Experimental Center of Shanxi Bethune Hospital provided the equipment for this study.

Funding

This study was supported by funding from the Beijing Science and Technology Innovation Medical Development Foundation (grant no. KC2023-JX-0186-RM075).

Availability of data and materials

The data generated in the present study may be requested from the corresponding author. The mass spectrometry proteomics data generated in the present study may be found in the ProteomeXchange Consortium and the PRIDE (42) partner repository under accession number PXD057462 or by using the URL: https://www.ebi.ac.uk/pride/archive/projects/PXD057462. The transcriptome data generated in the present study may be found in the Gene Expression Omnibus under accession number GSE280733 or by using the URL: https://www.ncbi.nlm.nih.gov/geo/query/acc.cgi?acc=GSE280733.

Authors' contributions

QZ designed the study, performed experiments, analyzed the data and wrote the manuscript. MW designed the study and performed experiments. SW conceived the study and wrote the manuscript. All authors read and approved the final version

of the manuscript. QZ, MW and SW confirm the authenticity of all the raw data.

Ethics approval and consent to participate

The study protocol was approved by the Ethics Committee of the Third Hospital of Shanxi Medical University (approval no. YXLL-2024-117). All participants provided written informed consent.

Patient consent for publication

Not applicable.

Competing interests

The authors declare that they have no competing interests.

References

1. Sung H, Ferlay J, Siegel RL, Laversanne M, Soerjomataram I, Jemal A and Bray F: Global cancer statistics 2020: GLOBOCAN estimates of incidence and mortality worldwide for 36 cancers in 185 countries. CA A Cancer J Clin 71: 209-249, 2021.
2. Chen W, Zheng R, Baade PD, Zhang S, Zeng H, Bray F, Jemal A, Yu XQ and He J: Cancer statistics in China, 2015. CA Cancer J Clin 66: 115-132, 2016.
3. Siegel RL, Giaquinto AN and Jemal A: Cancer statistics, 2024. CA Cancer J Clin 74: 12-49, 2024.
4. Xia C, Dong X, Li H, Cao M, Sun D, He S, Yang F, Yan X, Zhang S, Li N and Chen W: Cancer statistics in China and United States, 2022: Profiles, trends, and determinants. Chin Med J (Engl) 135: 584-590, 2022.
5. Monk BJ, Colombo N, Tewari KS, Dubot C, Caceres MV, Hasegawa K, Shapira-Frommer R, Salman P, Yañez E, Gümüş M, *et al*: First-line pembrolizumab + chemotherapy versus placebo + chemotherapy for persistent, recurrent, or metastatic cervical cancer: Final overall survival results of KEYNOTE-826. J Clin Oncol 41: 5505-5511, 2023.
6. Monk BJ, Tewari KS, Dubot C, Caceres MV, Hasegawa K, Shapira-Frommer R, Salman P, Yañez E, Gümüş M, Hurtado de Mendoza MO, *et al*: Health-related quality of life with pembrolizumab or placebo plus chemotherapy with or without bevacizumab for persistent, recurrent, or metastatic cervical cancer (KEYNOTE-826): A randomised, double-blind, placebo-controlled, phase 3 trial. Lancet Oncol 24: 392-402, 2023.
7. Kang I and Bucala R: The immunobiology of MIF: Function, genetics and prospects for precision medicine. Nat Rev Rheumatol 15: 427-437, 2019.
8. Zhao H, Wu L, Yan G, Chen Y, Zhou M, Wu Y and Li Y: Inflammation and tumor progression: Signaling pathways and targeted intervention. Signal Transduct Target Ther 6: 263, 2021.
9. Greten FR and Grivennikov SI: Inflammation and cancer: Triggers, mechanisms, and consequences. Immunity 51: 27-41, 2019.
10. Ravichandran KA and Heneka MT: Inflammasomes in neurological disorders-mechanisms and therapeutic potential. Nat Rev Neurol 20: 67-83, 2024.
11. Fu J, Schroder K and Wu H: Mechanistic insights from inflammasome structures. Nat Rev Immunol 24: 518-535, 2024.
12. Harris J, VanPatten S, Deen NS, Al-Abed Y and Morand EF: Rediscovering MIF: New tricks for an old cytokine. Trends Immunol 40: 447-462, 2019.
13. Liu Y, Liu Y, Wang Q, Song Y, Chen S, Cheng B, Zhang Y, Cui Z, Wu Z and Zhu C: MIF inhibitor ISO-1 alleviates severe acute pancreatitis-associated acute kidney injury by suppressing the NLRP3 inflammasome signaling pathway. Int Immunopharmacol 96: 107555, 2021.
14. Wu S, Lian J, Tao H, Shang H and Zhang L: Correlation of macrophage migration inhibitory factor gene polymorphism with the risk of early-stage cervical cancer and lymphatic metastasis. Oncol Lett 2: 1261-1267, 2011.
15. Tsuchiya S, Yamabe M, Yamaguchi Y, Kobayashi Y, Konno T and Tada K: Establishment and characterization of a human acute monocytic leukemia cell line (THP-1). Int J Cancer 26: 171-176, 1980.
16. Livak KJ and Schmittgen TD: Analysis of relative gene expression data using real-time quantitative PCR and the 2(-Delta Delta C(T)) method. Methods 25: 402-408, 2001.
17. Yang H, Xia L, Chen J, Zhang S, Martin V, Li Q, Lin S, Chen J, Calmette J, Lu M, *et al*: Stress-glucocorticoid-TSC22D3 axis compromises therapy-induced antitumor immunity. Nat Med 25: 1428-1441, 2019.
18. Nataraja C, Flynn J, Dankers W, Northcott M, Zhu W, Sherlock R, Bennett TJ, Russ BE, Miceli I, Pervin M, *et al*: GILZ regulates type I interferon release and sequesters STAT1. J Autoimmun 131: 102858, 2022.
19. Flamini S, Sergeev P, Viana de Barros Z, Mello T, Biagioli M, Paglialunga M, Fiorucci C, Prikazchikova T, Pagano S, Gagliardi A, *et al*: Glucocorticoid-induced leucine zipper regulates liver fibrosis by suppressing CCL2-mediated leukocyte recruitment. Cell Death Dis 12: 421, 2021.
20. Ma Y, Yang H and Kroemer G: Endogenous and exogenous glucocorticoids abolish the efficacy of immune-dependent cancer therapies. Oncoimmunology 9: 1673635, 2020.
21. de Visser KE and Joyce JA: The evolving tumor microenvironment: From cancer initiation to metastatic outgrowth. Cancer Cell 41: 374-403, 2023.
22. Mellman I, Chen DS, Powles T and Turley SJ: The cancer-immunity cycle: Indication, genotype, and immunotype. Immunity 56: 2188-2205, 2023.
23. Ochando J, Mulder WJM, Madsen JC, Netea MG and Duivenvoorden R: Trained immunity-basic concepts and contributions to immunopathology. Nat Rev Nephrol 19: 23-37, 2023.
24. Kloosterman DJ and Akkari L: Macrophages at the interface of the co-evolving cancer ecosystem. Cell 186: 1627-1651, 2023.
25. Pittet MJ, Michielin O and Migliorini D: Clinical relevance of tumour-associated macrophages. Nat Rev Clin Oncol 19: 402-421, 2022.
26. Locati M, Curtale G and Mantovani A: Diversity, mechanisms, and significance of macrophage plasticity. Annu Rev Pathol 15: 123-147, 2020.
27. Wang H, Yung MMH, Ngan HYS, Chan KKL and Chan DW: The impact of the tumor microenvironment on macrophage polarization in cancer metastatic progression. Int J Mol Sci 22: 6560, 2021.
28. Anderson NR, Minutolo NG, Gill S and Klichinsky M: Macrophage-based approaches for cancer immunotherapy. Cancer Res 81: 1201-1208, 2021.
29. Bian Z, Gong Y, Huang T, Lee CZW, Bian L, Bai Z, Shi H, Zeng Y, Liu C, He J, *et al*: Deciphering human macrophage development at single-cell resolution. Nature 582: 571-576, 2020.
30. Woolbright BL, Rajendran G, Abbott E, Martin A, Amalraj S, Dennis K, Li X, Warrick J and Taylor JA III: Role of MIF1/MIF2/CD74 interactions in bladder cancer. J Pathol 259: 46-55, 2022.
31. Huang G, Ma L, Shen L, Lei Y, Guo L, Deng Y and Ding Y: MIF/SCL3A2 depletion inhibits the proliferation and metastasis of colorectal cancer cells via the AKT/GSK-3β pathway and cell iron death. J Cell Mol Med 26: 3410-3422, 2022.
32. Jia X, Xi J, Tian B, Zhang Y, Wang Z, Wang F, Li Z, Long J, Wang J, Fan GH and Li Q: The tautomerase activity of tumor exosomal MIF promotes pancreatic cancer progression by modulating MDSC differentiation. Cancer Immunol Res 12: 72-90, 2024.
33. Penticuff JC, Woolbright BL, Sielecki TM, Weir SJ and Taylor JA: MIF family proteins in genitourinary cancer: Tumorigenic roles and therapeutic potential. Nat Rev Urol 16: 318-328, 2019.
34. Wang Q, Wei Y and Zhang J: Combined knockdown of D-dopachrome tautomerase and migration inhibitory factor inhibits the proliferation, migration, and invasion in human cervical cancer. Int J Gynecol Cancer 27: 634-642, 2017.
35. Cao X and Xu J: Insights into inflammasome and its research advances in cancer. Tumori 105: 456-464, 2019.
36. Barnett KC, Li S, Liang K and Ting JPY: A 360° view of the inflammasome: Mechanisms of activation, cell death, and diseases. Cell 186: 2288-2312, 2023.
37. Ershaid N, Sharon Y, Doron H, Raz Y, Shani O, Cohen N, Monteran L, Leider-Trejo L, Ben-Shmuel A, Yassin M, *et al*: NLRP3 inflammasome in fibroblasts links tissue damage with inflammation in breast cancer progression and metastasis. Nat Commun 10: 4375, 2019.

38. Kopalli SR, Kang TB, Lee KH and Koppula S: NLRP3 Inflammasome activation inhibitors in inflammation-associated cancer immunotherapy: An update on the recent patents. Recent Pat Anticancer Drug Discov 13: 106-117, 2018.
39. Wang L, Wang C, Tao Z, Zhu W, Su Y and Choi WS: Tumor-associated macrophages facilitate oral squamous cell carcinomas migration and invasion by MIF/NLRP3/IL-1β circuit: A crosstalk interrupted by melatonin. Biochim Biophys Acta Mol Basis Dis 1869: 166695, 2023.
40. Basak U, Sarkar T, Mukherjee S, Chakraborty S, Dutta A, Dutta S, Nayak D, Kaushik S, Das T and Sa G: Tumor-associated macrophages: An effective player of the tumor microenvironment. Front Immunol 14: 1295257, 2023.
41. Figueiredo CR, Azevedo RA, Mousdell S, Resende-Lara PT, Ireland L, Santos A, Girola N, Cunha RLOR, Schmid MC, Polonelli L, *et al*: Blockade of MIF-CD74 signalling on macrophages and dendritic cells restores the antitumour immune response against metastatic melanoma. Front Immunol 9: 1132, 2018.
42. Perez-Riverol Y, Bai J, Bandla C, García-Seisdedos D, Hewapathirana S, Kamatchinathan S, Kundu DJ, Prakash A, Frericks-Zipper A, Eisenacher M, *et al*: The PRIDE database resources in 2022: A hub for mass spectrometry-based proteomics evidences. Nucleic Acids Res 50: D543-D552, 2022.